Applied Physics Letters

A hybrid (Al)GaAs-$LiNbO_3$ surface acoustic wave resonator for cavity quantum dot optomechanics

Cite as: Appl. Phys. Lett. **117**, 121106 (2020); https://doi.org/10.1063/5.0022542
Submitted: 21 July 2020 . Accepted: 10 September 2020 . Published Online: 25 September 2020

Emeline D. S. Nysten, Armando Rastelli, and Hubert J. Krenner

AIP Publishing

Applied Physics Letters ARTICLE scitation.org/journal/apl

A hybrid (Al)GaAs-$LiNbO_3$ surface acoustic wave resonator for cavity quantum dot optomechanics

Cite as: Appl. Phys. Lett. **117**, 121106 (2020); doi: 10.1063/5.0022542
Submitted: 21 July 2020 · Accepted: 10 September 2020 ·
Published Online: 25 September 2020

Emeline D. S. Nysten,[1] Armando Rastelli,[2] and Hubert J. Krenner[1,a)]

AFFILIATIONS

[1]Lehrstuhl für Experimentalphysik 1 and Augsburg Centre for Innovative Technologies (ACIT), Universität Augsburg, Universitätsstraße 1, 86159 Augsburg, Germany
[2]Institute of Semiconductor and Solid State Physics, Johannes Kepler Universität Linz, Linz Institute of Technology, Altenbergerstraße 69, 4040 Linz, Austria

Note: This paper is part of the Special Issue on Hybrid Quantum Devices.
[a)]**Author to whom correspondence should be addressed:** hubert.krenner@physik.uni-augsburg.de

ABSTRACT

A hybrid device comprising a (Al)GaAs quantum dot heterostructure and a $LiNbO_3$ surface acoustic wave resonator is fabricated by heterointegration. High acoustic quality factors $Q > 4000$ are demonstrated for an operation frequency $f \approx 300$ MHz. The measured large quality factor-frequency products $Q \times f > 10^{12}$ ensure the suppression of decoherence due to thermal noise for temperatures exceeding $T > 50$ K. Frequency and position dependent optomechanical coupling of single quantum dots and resonator modes is observed.

Elastic waves and acoustic phonons are known to couple to literally any excitation in condensed matter. This unique property makes them ideally suited for the design and realization of hybrid quantum systems.[1] Recently, surface acoustic waves (SAWs),[2] i.e., surface-confined elastic waves, shifted back into the focus of this active field of research. These coherent radio frequency (rf) phonons enable versatile quantum transduction[3] and dynamic, non-adiabatic control of quantum systems.[4] In experiment, the SAWs have been employed for the coherent control of superconducting qubits in the single phonon limit,[5] on-chip quantum state transfer between superconducting qubits by single SAW quanta,[6] single electron spin transfer between electrostatic quantum dots (QDs),[7] and coherent acoustic control of single spins,[8,9] defect centers,[10,11] and optically active QDs.[12–15] Optically active, epitaxial QDs exhibit distinct advantages for the design of hybrid quantum architectures. Their emission wavelength can be tuned by chemical composition and size[16] or post-growth by external parameters such as electric or magnetic fields[17] or strain.[18] In addition, the tunable coupling can be achieved between excitons in multi-dot architectures[19,20] and excitons and optical modes in photonic systems.[21,22] In SAW technology and nonlinear optics, Lithium Niobate ($LiNbO_3$)[23] is the substrate material of choice because of its high electromechanical coupling coefficient $K^2 \approx 5\%$ ($K^2 \approx 0.07\%$ for GaAs) and $\chi^{(2)}$ ($\chi^{(2)} = 0$ for GaAs) optical nonlinearity, respectively. Because $LiNbO_3$ does not provide any type of high-quality qubit system, the design and fabrication of hybrid quantum devices requires its heterointegration with other materials. Here, we report on the realization of a hybrid SAW resonator device comprising a SAW cavity defined on a $LiNbO_3$ substrate and epitaxially grown optically active QDs. We demonstrate optomechanical coupling of single QDs to the phononic modes of the resonator. This coupling is determined by the local amplitude of the acoustic field at the QD's position. Interestingly, the QD's optomechanical response exhibits a richer spectrum than the electrically determined resonator properties, opening new directions for future explorations employing our hybrid device.

Our device is fabricated by heterointegration of a (Al)GaAs heterostructure containing a single layer of droplet etched QDs onto a conventional single port $LiNbO_3$ SAW resonator device.[24] A schematic of our device is shown in Fig. 1(a). The SAW resonator is patterned onto a oxygen-reduced 128° rotated Y-cut $LiNbO_{3-x}$ substrate. The resonator is formed by two metallic floating electrode acoustic Bragg-reflectors (150 fingers, aperture $a = 350\,\mu$m, nominal mirror separation $d = 4522\,\mu$m) and is aligned along the X-direction. The phase velocity of the SAW is $c_{SAW,0} = 3990$ m/s along this direction. The nominal acoustic design wavelength and frequency are $\bar{\lambda}_n = 13.3\,\mu$m and $\bar{f}_n = 300$ MHz, respectively. The resonator is excited by applying

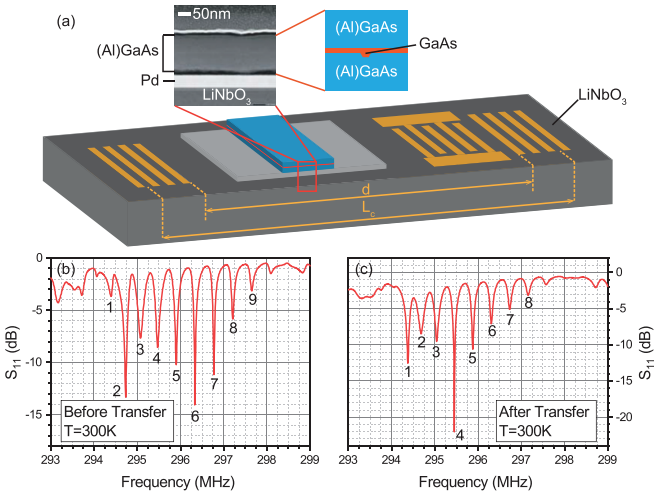

FIG. 1. (a) Schematic of the hybrid device comprising a $LiNbO_3$ single port SAW resonator and a (Al)GaAs heterostructure containing a single layer of QDs on a Pd adhesion layer. The inset shows a TEM image of the $LiNbO_3$-Pd-(Al)GaAs stack. Measured room temperature rf reflectivity (S_{11}) of the SAW resonator before (b) and after (c) heterointegration of the QD layer.

an electrical rf signal of frequency f_{rf} to a 20 finger pairs interdigital transducer (IDT). The acoustic Bragg mirrors and the IDT are patterned during the same electron beam lithography step and finalized using a Ti (5 nm)/Al (50 nm) metallization in a lift-off process. The IDT is positioned off-center, close to one Bragg mirror and the large open area is used for the heterointegration of the III–V compound semiconductor film. Figure 1(b) shows the rf reflectivity of our resonator device measured with the IDT at $T = 300$ K. In this spectrum, we can identify nine pronounced phononic modes, which are consecutively numbered. The measured complex reflection $S_{11}(f)$ can be fitted by[25]

$$\tilde{S}_{11}(f) = \frac{(Q_e - Q_{i,n})/Q_e + 2iQ_{i,n}(f - f_n)/f}{(Q_e + Q_{i,n})/Q_e + 2iQ_{i,n}(f - f_n)/f}. \quad (1)$$

In this expression, $Q_{i,n}$ and Q_e denote the internal and external quality factor of mode n and external circuit, respectively. f_n is the resonance frequency of the n-th mode. We find a mean $\overline{Q}_i = 2900 \pm 700$ ($\overline{\Delta f} = 100 \pm 20$ kHz) and $\overline{f}_n = 296$ MHz at room temperature. The given values are the mean of the distribution and their standard deviation from the mean. The full analysis is included in the supplementary material. These modes are split by the free spectral length $FSR_{empty} = 416 \pm 25$ kHz. This value corresponds to a cavity round trip time of $T_c = \frac{1}{FSR} = 2.41 \pm 0.15\ \mu$s and a resonator length $L_c = \frac{c_{SAW,0}}{2FSR} = 4800 \pm 50\ \mu$m. The penetration length of the acoustic field into the mirror is given by $L_p = w/|r_s| = 145\ \mu$m, where $w = 3.3\ \mu$m is the width of the fingers of the mirror and $r_s = 0.023$ is the reflectivity coefficient of one finger.[25,26] Using the lithographically defined d, we calculate a resonator length $d + 2L_p = 4810\ \mu$m, which agrees well with the value derived from the experimental data. The heterointegration is realized by epitaxial lift-off and transfer onto a 50 nm thick and 3000 μm long Pd adhesion layer.[27–31] The heterostructure was grown by molecular beam epitaxy and consists of a 150 nm thick $Al_{0.33}Ga_{0.67}As$ membrane with a layer of strain-free GaAs QDs[32] in its center. The membrane was heterointegrated onto the $LiNbO_3$ SAW-resonator by epitaxial lift-off and transfer. In essence, the QD heterostructure is released from the growth substrate by selective etching of an $Al_{0.75}Ga_{0.25}As$ sacrificial layer using hydrofluoric acid. In the next step, the membrane is transferred onto the Pd adhesion layer in the center of the SAW resonator and a rectangular piece is isolated by wet-chemical etching. Further details can be found in Ref. 29 and the supplementary material. A transmission electron microscope (TEM) image of the $LiNbO_3$-Pd-(Al)GaAs stack is shown in Fig. 1(a). The semiconductor membrane is laterally placed in the center of the resonator. After transfer, the membrane is etched to obtain straight edges and, thus, reduce scattering losses. The final membrane is 215 μm wide and extends over the full width of the resonator. Further details on the heterostructure and an optical microscopy image are included in the supplementary material. The resonator mode spectrum after transfer recoded at $T = 300$ K is shown in Fig. 1(c) and is analyzed using Eq. (1). The full analysis is also part of the supplementary material. By comparing these data to those before transfer, we find that the mode spectrum and FSR remain approximately constant within the experimental error at $\overline{f}_n = 295.8$ MHz and $FSR_{hybrid} = 406 \pm 22$ kHz. The corresponding cavity round trip time is $T_{c,hybrid} = 2.46 \pm 0.13\ \mu$s. Most importantly, high internal quality factors of $\overline{Q}_i = 2500 \pm 300$ ($\overline{\Delta f} = 120 \pm 15$ kHz) are preserved after transfer, which is of highest relevance for strong phonon-exciton coupling. Furthermore, all experimental data are well reproduced by finite element modelling (FEM) detailed in the supplementary material. For example, the experimental change of T_c after heterointegration of $\Delta T_c = 50$ ns is in excellent agreement with the 60 ns predicted by FEM. Furthermore, the reduction of the effective phase velocity in the hybridized region to $c_{SAW,eff} = 3889$ m/s gives rise to a spectral shift of the mode spectrum of $\Delta f_n = 10.5$ MHz to lower frequencies. Note, that according to these calculations, the absolute mode index changes from $n_{abs,0} = n + 707$ of the bare resonator to $n_{abs,eff} = n + 726$, for the hybrid device.

Next, we investigate the optomechanical coupling of single QDs to the phononic modes of the resonator in Fig. 2. The dominant coupling mechanism is deformation potential coupling, i.e., the modulation of the semiconductor's bandgap by hydrostatic pressure, i.e., normal stress.[15] The Pd adhesion layer effectively shortens any electric field.[29,30] Thus, Stark effect modulation, which becomes dominant at high SAW amplitudes,[33] is to be strongly suppressed. We measure the optomechanical response at low temperatures ($T = 10$ K) by time and phase averaged micro-photoluminescence spectroscopy.[15] Importantly, we record the reflected electrical power ($P_{reflected}$) at every step, i.e., for any combination of electrical frequency (f_{rf}) and power (P_{rf}) applied to the IDT. Thus, we eliminate potential sources of errors for instance due to temperature related drifts of the mode spectrum. Further details can be found in the supplementary material. In essence, the detected line shape is a time-average of the dynamic optomechanical modulation of the unperturbed, Lorentzian QD emission line.[33] In a first step, we apply $P_{rf} = 5$ dBm to the IDT at $f_5 = 300.25$ MHz. The measured $P_{reflected}$ is plotted as a function of f_{rf} in the inset of Fig. 2(a). The main panel shows the emission spectra of two QDs, QD1 and QD2 with (red) and without (black) the SAW resonating in the cavity. The two QDs are separated by $\simeq 21\ \mu$m $\simeq 1.6\ \lambda_{SAW}$ along the cavity axis and exhibit completely dissimilar behavior. While QD1 shows a pronounced broadening when the SAW is generated, the line shape of QD2, apart from a weak reduction of the overall intensity

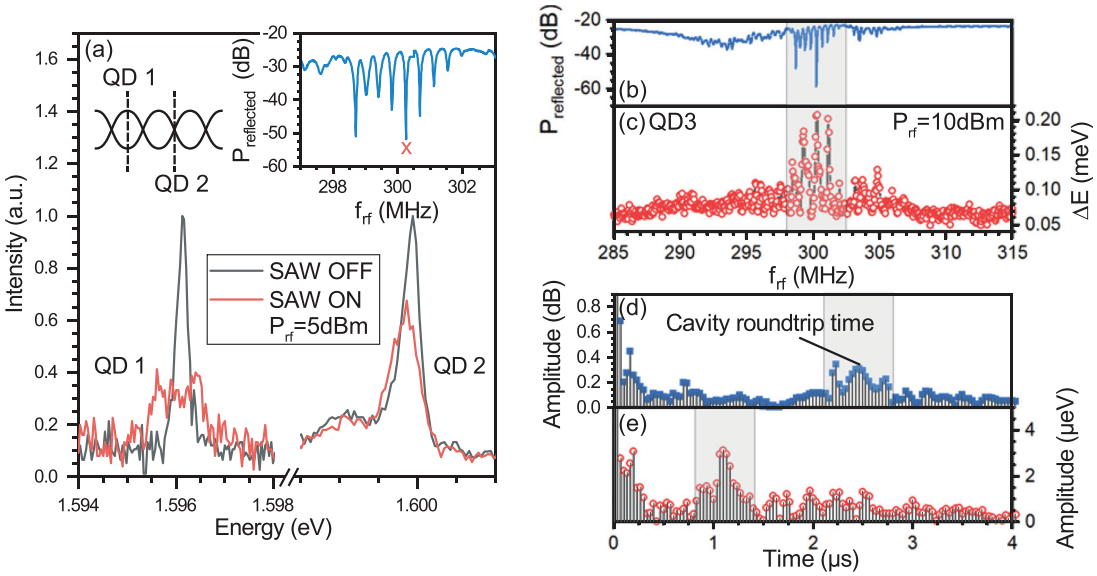

FIG. 2. (a) Low temperature emission spectra of two QDs inside the SAW resonator without (black lines) and with (red lines) $f_{rf} = 300.25$ MHz applied with $P_{rf} = 5$ dBm to the IDT. This applied frequency is resonant to the $n = 5$ mode marked in the measured reflected power spectrum of the resonator (inset). QD1 (QD2) is located close or at an antinode (a node) of the cavity field as shown by the schematic. (b) Reflected power spectrum and (c) simultaneous optomechanical response of QD3. (d) and (e) FFT of the data in (b) and (c) showing a clear signature at T_c and $T_c/2$, respectively.

remains unaffected. These types of behaviors are expected for QDs positioned at an antinode (QD1) or node (QD2) of the acoustic cavity field. From the observed optomechanical responses, we infer that QD1 and QD2 are located at an antinode or node of the mode, respectively, as illustrated by the schematic. In a second step, we keep the optical excitation fixed and scan the radio frequency f_{rf} applied at a constant power level over a wide range of frequencies 285−315 MHz and record the emission spectra of a single QD (QD3). These data are fitted with a time-integrated, sinusoidally modulated Lorentzian[29,34] of width w and amplitude A.

$$I(E) = I_0 + f_{rf}\frac{2A}{\pi}\int_0^{1/f_{rf}} \frac{w}{4\cdot\left(E-\left(E_0+\Delta E\cdot\sin\left(2\pi\cdot f_{rf}\cdot t\right)\right)\right)^2+w^2}dt. \tag{2}$$

In Eq. (2), E_0 and ΔE denote the center energy of the emission peak and the optomechanical modulation amplitude due to the time-dependent deformation potential coupling. From our established FEM modelling[29] we obtain an optomechanical coupling parameter[14,15] $\gamma_{om} = 2500\,\mu$eV/nm. Moreover, the measured ΔE per repetition of the IDT pattern is enhance by at least a factor of 2 when compared to the previously studied delay line device.[29] Figures 2(b) and 2(c) show the simultaneously recorded reflected rf power ($P_{reflected}$) and ΔE as a function of f_{rf}. Clearly, QD3 exhibits a series of strong optomechanical modulation peaks at frequencies at which pronounced cavity modes are observed (grey shaded area). This observation of a pronounced coupling to resonator modes is a first direct evidence of cavity enhanced coupling between SAW phonons and the exciton transition of a single QD. However, the detected optomechanical response, $\Delta E(f_{rf})$, of QD3 exhibits noticeably less peaks than $P_{reflected}$. We Fast Fourier transform (FFT) $P_{reflected}(f_{rf})$ and $\Delta E(f_{rf})$ to obtain time domain information. The result of these Fourier transform is plotted in Figs. 2(d) and 2(e). In the FFT of $P_{reflected}(f_{rf})$ in (d), a clear peak at $t = 2.4 \pm 0.05\,\mu$s can be identified, which matches exactly the cavity round trip time, $T_c = 2.41\,\mu$s of the SAW resonator derived from the measured *FSR*. In contrast, the FFT of $\Delta E(f_{rf})$ in (e) shows a clear signal at $t = 1.1 \pm 0.1\,\mu\text{s} \simeq T_c/2$. This apparent halving of the round trip time, i.e., doubling of the *FSR*, in the dot's optomechanical response provides first direct evidence that coupling occurs only to every second cavity mode.

We continue studying this mode index selective coupling in more detail. In Fig. 3, we investigate the f_{rf}-dependence of the optomechanical response of QD3 and another different dot, QD4, in (a) and (b), respectively. The main panels show the optomechanical modulation amplitude ΔE derived from the best fits of Eq. (2) and the upper panels show the simultaneously measured $P_{reflected}$. All data are plotted as a function of the frequency shift with respect to the center mode $n = 5$. From these electrical data, we obtain the low temperature value of the mean quality factor $\overline{Q} = 4430 \pm 1560$, an increase by a factor of ≈1.75 compared to the room temperature value. Furthermore, we analyze the quality factor-frequency product $(Q \times f)$, a commonly used figure of merit to compare mechanical resonators.[35] Here, we obtain $\overline{Q} \times f = (1.33 \pm 0.48) \cdot 10^{12}$, which in the quantum realm has to be compared to the thermal energy. In our case, the SAW phonon energy of ≈1.25 μeV is less than $k_BT \approx 250\,\mu$eV and the maximum number of coherent oscillations, i.e., number of coherent operations possible, is limited by thermal decoherence to $Q \times f \times \frac{h}{k_BT}$. At $T = 10$ K, thermal decoherence limits the number of coherent oscillations[36] in the unloaded hybrid resonator device to $\overline{Q} \times f \times \frac{h}{k_BT} \approx 6$. A single oscillation will be preserved even up to 50 K. QD3 shows a strong optomechanical response when modes with an odd index $n = 5, 7$ are excited. In contrast, QD4

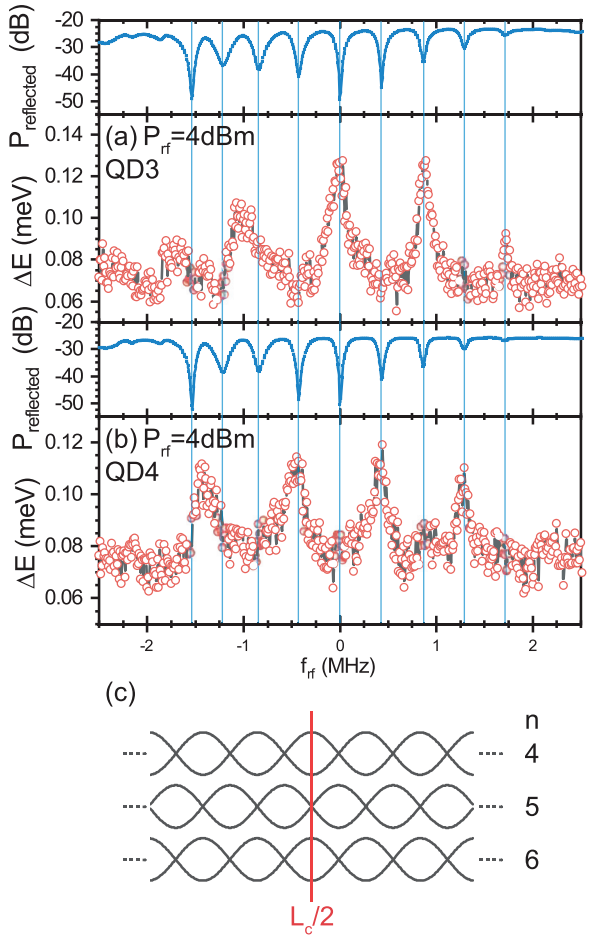

FIG. 3. rf-dependent optomechanical response of QD3 (a) and QD4 (b) measured at $T = 10\,K$. Upper panels: reflected rf power $P_{reflected}$. Main panels: optomechanical response $\Delta E\,(f_{rf})$. (c) Schematic of the acoustic field in the center of the resonator for the modes detected in the experimental data above.

couples to modes with an even index $n = 4, 6, 8$. The width of these resonances corresponds to an optomechanically detected quality factor $\overline{Q_{QD}} = 1730 \pm 420$ ($\overline{\Delta f_{QD}} = 890 \pm 30$ kHz). This decrease compared to the electrically measured value may arise from imperfections during heterointegration, e.g., inhomogeneous bonding and roughness and misalignment of the etched edges. Moreover, the splitting between modes which optomechanically couple to the QD is doubled compared to the *FSR* measured electrically, and consequently, the corresponding time is half of the cavity round trip time. The alternating coupling behavior can be understood well considering the position of nodes and antinodes of the acoustic fields of different modes in the center of the resonator. The qualitative profiles of the $n = 4$, 5, and 6 are shown in Fig. 3(c). Clearly, modes with an even (odd) index exhibit nodes (antinodes). Thus, a single QD positioned at nodes or antinodes can be selectively coupled to modes with either an even or odd mode index, and QD3 and QD4 are two representative examples for each case. This simple picture applies well to modes $n \geq 4$. For $n \leq 3$, a more complex behavior is observed. For QD4, we observe a strong optomechanical response at $(f_2 + f_1)/2$, and for QD3, similarly at $(f_3 + f_2)/2$. At the same time, no optomechanical response is detected for $n = 1$ and $n = 3$, and for $n = 2$, expected for QD3 and QD4, respectively. For linear optomechanical coupling between the resonating SAW and the QD, a pronounced optomechanical response should be detected only when the driving rf signal is in resonance with modes of odd (QD3) and even (QD4) index. Moreover, no optomechanical response should be detected when f_{rf} is detuned from a cavity mode because the large cavity efficiently rejects phonons in this case. Despite the fact that the acoustic power injected in the resonator remains finite in a real, lossy device like ours, the observed behavior cannot be attributed to simple, linear coupling mediated by the deformation potential. In the supplementary material, we show data from another QD5. This dot is heterointegrated in a different, nominally identical SAW resonator. QD5 shows identical optomechanical response as QD3, thus these data corroborate that the observations made are reproducible for this type of device. This in particular, excludes that the observation can be solely attributed to local imperfections. As shown in Fig. 4(a), the optical linewidth of the QD[37] $\Gamma_{QD} \sim 1.25$ GHz, fully covers the entire phononic mode spectrum. Thus, coupling between all phononic modes can occur. Figures 4(b)–4(d) compare the measured optomechanical response of QD3 for three different P_{rf}. The full analysis is included in the supplementary material. The reflected rf power is given as a reference in the upper panels. As P_{rf} increases, the optomechanical modulation amplitude ΔE of QD3 increases and, moreover, new features develop, which are not observed for a low P_{rf} in Fig. 3(b). The reflected electrical power spectra in the upper panels do not show similar pronounced changes which indicates that there is no strong backaction and transduction to the acoustic domain. Most notably, at the highest power level applied to the IDT, i.e., the maximum number of phonons injected into the resonator, $P_{rf} = 16$ dBm, we observe clearly resolved new features at $(f_4 + f_3)/2$ and $(f_6 + f_5)/2$. Again, in an ideal device and for coupling mediated by the deformation potential, these features are completely unexpected. We study the dependence of the optomechanical modulation on P_{rf}. Such f_{rf}-scans were recorded for nine different P_{rf}. We extracted the maximum of the optomechanical modulation amplitude ΔE_{max} at $(f_3 + f_2)/2$ (1, black), f_5 (2, red), and f_7 (3, blue). The data are plotted as symbols in logarithmic representation as a function of P_{rf} in Fig. 4(e) to identify power law dependencies. The lines in Fig. 4(e) are linear fits to the data from which we are able to determine the power law for the three selected frequencies. Clearly, $(f_3 + f_2)/2$ (1, black), f_5 (2, red), and f_7 (3, blue) exhibit power law dependences with slopes $m_1 = 0.85 \pm 0.1$, $m_2 = 0.7 \pm 0.1$, and $m_3 = 0.75 \pm 0.1$, respectively. These exponents are greater than $\Delta E_{max} \propto P_{rf}^{1/2}$ for linear deformation potential coupling, as observed in similar hybrid devices for propagating SAWs.[29,30] It is also less than $\Delta E_{max} \propto P_{rf}^{1}$, expected for Stark-effect modulation, which however, can be excluded in our device.

In conclusion, we demonstrate the heterointegration of an (Al)GaAs based QD-heterostructure on a $LiNbO_3$ SAW resonator. In our hybrid device, we demonstrate strong optomechanical coupling between single QDs with the phononic modes of the SAW-resonator. This coupling is position dependent determined by the spatial overlap of the acoustic field and the QD. Our platform represents an important step towards hybrid semiconductor-$LiNbO_3$ quantum devices. In particular, our approach is fully compatible with emerging thin film

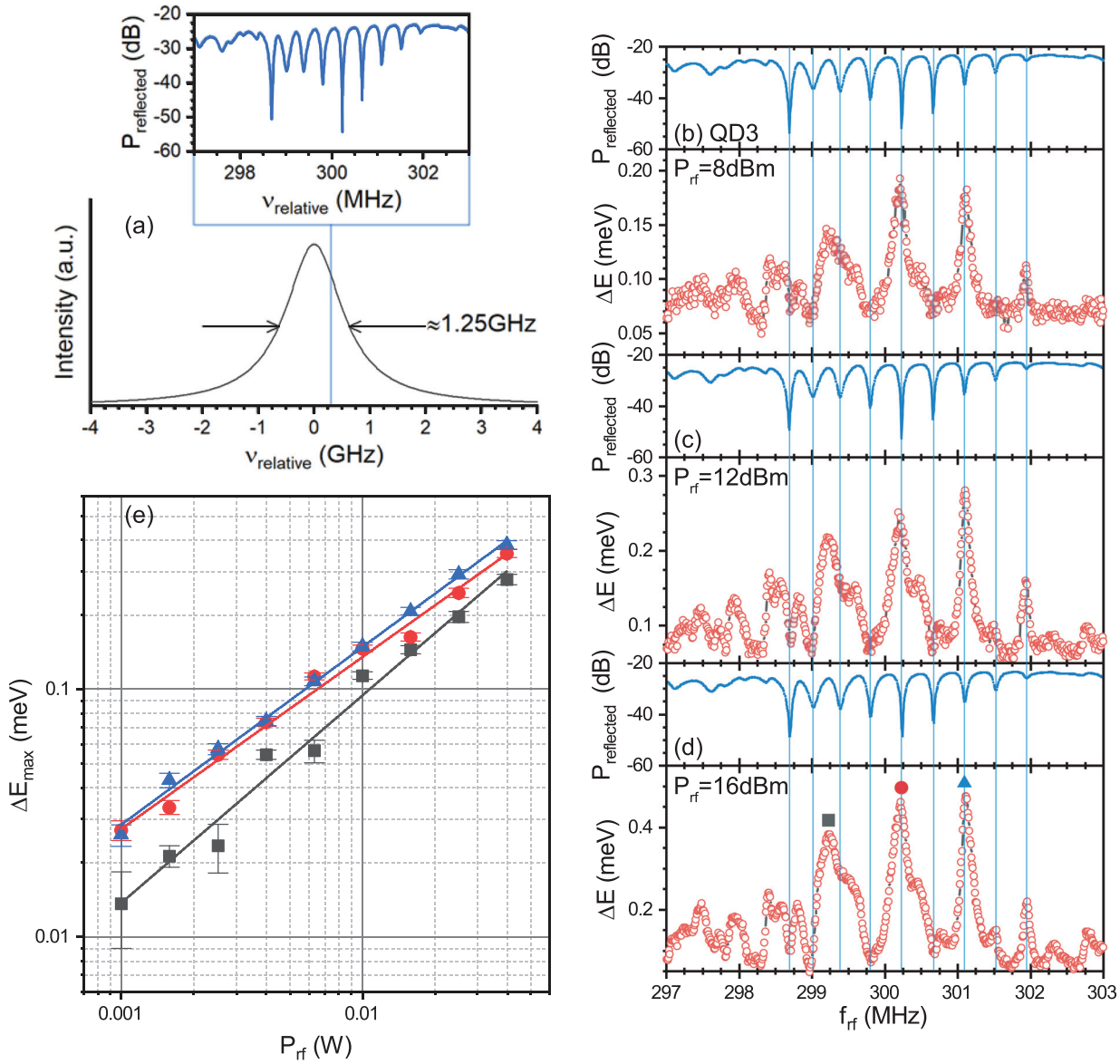

FIG. 4. (a) Schematic showing the linewidth of the QD in comparison to the phononic spectrum of the resonator. (b)–(d) Optomechanical response of QD3 for three selected values of P_{rf} 8 (b), 12 (c), and 16 dBm (d) (main panels). Upper panels show the simultaneously measured $P_{reflected}$. (e) Amplitudes of three selected peaks [marked by corresponding symbols in (d)] as a function of P_{rf}.

$LiNbO_3$ technology[38–41] and a wide variety of quantum emitters.[42] Moreover, it can be readily combined with electrical contacts[30] facilitating quasi-static Stark-tuning of the QD's optical transitions. Finally, small mode volume and high frequency (>1 GHz) resonators may enable coherent optomechanical control in the resolved sideband regime which has been reached both for III–V QDs[13,43] and defect centers.[10] These advancements may allow to unravel the physical origin of the complex optomechanical coupling observed for certain frequencies and at high acoustic drive amplitudes. Finally, the demonstrated hybrid architecture promises a strong enhancement of the optomechanical coupling compared to traditional monolithic approaches.[44]

See the supplementary material for the sample design, details on the optical experiments, rf characterization, FEM, additional experimental data of QD5, and best fits of the data in Fig. 4.

This project has received funding from the European Union's Horizon 2020 research and innovation programme under the Marie Sklodowska-Curie Grant Agreement No. 642688 (SAWtrain), and

the Deutsche Forschungsgemeinschaft (DFG) via the Cluster of Excellence "Nanosystems Initiative Munich" (NIM), the Austrian Science Fund (FWF): P 29603, I 4320, the Linz Institute of Technology (LIT), and the LIT Lab for secure and correct systems, supported by the State of Upper Austria. We thank Maximilian Gnedel and Ferdinand Haider for performing TEM and Achim Wixforth for his continuous support and invaluable discussions.

DATA AVAILABILITY

The data that support the findings of this study are available from the corresponding author upon reasonable request.

REFERENCES

[1]G. Kurizki, P. Bertet, Y. Kubo, K. Mølmer, D. Petrosyan, P. Rabl, and J. Schmiedmayer, Proc. Natl. Acad. Sci. U.S.A. **112**, 3866 (2015).
[2]P. Delsing, A. N. Cleland, M. J. A. Schuetz, J. Knörzer, G. Giedke, J. I. Cirac, K. Srinivasan, M. Wu, K. C. Balram, C. Bäuerle, T. Meunier, C. J. B. Ford, P. v Santos, E. Cerda-Méndez, H. Wang, H. J. Krenner, E. D. S. Nysten, M. Weiß, G. R. Nash, L. Thevenard, C. Gourdon, P. Rovillain, M. Marangolo, J.-Y. Duquesne, G. Fischerauer, W. Ruile, A. Reiner, B. Paschke, D. Denysenko, D. Volkmer, A. Wixforth, H. Bruus, M. Wiklund, J. Reboud, J. M. Cooper, Y. Fu, M. S. Brugger, F. Rehfeldt, and C. Westerhausen, J. Phys. D: Appl. Phys. **52**, 353001 (2019).
[3]M. J. A. Schuetz, E. M. Kessler, G. Giedke, L. M. K. Vandersypen, M. D. Lukin, and J. I. Cirac, Phys. Rev. X **5**, 031031 (2015).
[4]R. Blattmann, H. J. Krenner, S. Kohler, and P. Hänggi, Phys. Rev. A **89**, 012327 (2014).
[5]M. V. Gustafsson, T. Aref, A. F. Kockum, M. K. Ekstrom, G. Johansson, and P. Delsing, Science **346**, 207 (2014).
[6]A. Bienfait, K. J. Satzinger, Y. P. Zhong, H.-S. Chang, M.-H. Chou, C. R. Conner, É. Dumur, J. Grebel, G. A. Peairs, R. G. Povey, and A. N. Cleland, Science **364**, 368 (2019).
[7]S. Takada, H. Edlbauer, H. v Lepage, J. Wang, P.-A. Mortemousque, G. Georgiou, C. H. W. Barnes, C. J. B. Ford, M. Yuan, P. v Santos, X. Waintal, A. Ludwig, A. D. Wieck, M. Urdampilleta, T. Meunier, and C. Bäuerle, Nat. Commun. **10**, 4557 (2019).
[8]S. J. Whiteley, G. Wolfowicz, C. P. Anderson, A. Bourassa, H. Ma, M. Ye, G. Koolstra, K. J. Satzinger, M. v Holt, F. J. Heremans, A. N. Cleland, D. I. Schuster, G. Galli, and D. D. Awschalom, Nat. Phys. **15**, 490 (2019).
[9]S. Maity, L. Shao, S. Bogdanović, S. Meesala, Y.-I. Sohn, N. Sinclair, B. Pingault, M. Chalupnik, C. Chia, L. Zheng, K. Lai, and M. Lončar, Nat. Commun. **11**, 193 (2020).
[10]D. A. Golter, T. Oo, M. Amezcua, K. A. Stewart, and H. Wang, Phys. Rev. Lett. **116**, 143602 (2016).
[11]S. Lazić, A. Espinha, S. Pinilla Yanguas, C. Gibaja, F. Zamora, P. Ares, M. Chhowalla, W. S. Paz, J. J. P. Burgos, A. Hernández-Mínguez, P. v Santos, and H. P. van der Meulen, Commun. Phys. **2**, 113 (2019).
[12]J. R. Gell, M. B. Ward, R. J. Young, R. M. Stevenson, P. Atkinson, D. Anderson, G. A. C. Jones, D. A. Ritchie, and A. J. Shields, Appl. Phys. Lett. **93**, 081115 (2008).
[13]M. Metcalfe, S. M. Carr, A. Muller, G. S. Solomon, and J. Lawall, Phys. Rev. Lett. **105**, 37401 (2010).
[14]F. J. R. Schülein, E. Zallo, P. Atkinson, O. G. Schmidt, R. Trotta, A. Rastelli, A. Wixforth, and H. J. Krenner, Nat. Nanotechnol. **10**, 512 (2015).
[15]M. Weiß and H. J. Krenner, J. Phys. D: Appl. Phys. **51**, 373001 (2018).
[16]J. M. García, T. Mankad, P. O. Holtz, P. J. Wellman, and P. M. Petroff, Appl. Phys. Lett. **72**, 3172 (1998).
[17]M. Bayer, G. Ortner, O. Stern, A. Kuther, A. A. Gorbunov, A. Forchel, P. Hawrylak, S. Fafard, K. Hinzer, T. L. Reinecke, S. N. Walck, J. P. Reithmaier, F. Klopf, and F. Schäfer, Phys. Rev. B **65**, 195315 (2002).
[18]R. Trotta, P. Atkinson, J. D. Plumhof, E. Zallo, R. O. Rezaev, S. Kumar, S. Baunack, J. R. Schröter, A. Rastelli, and O. G. Schmidt, Adv. Mater. **24**, 2668 (2012).
[19]E. A. Stinaff, M. Scheibner, A. S. Bracker, I. v Ponomarev, V. L. Korenev, M. E. Ware, M. F. Doty, T. L. Reinecke, and D. Gammon, Science **311**, 636 (2006).
[20]H. J. Krenner, E. C. Clark, T. Nakaoka, M. Bichler, C. Scheurer, G. Abstreiter, and J. J. Finley, Phys. Rev. Lett. **97**, 076403 (2006).
[21]A. Laucht, F. Hofbauer, N. Hauke, J. Angele, S. Stobbe, M. Kaniber, G. Böhm, P. Lodahl, M. Amann, and J. J. Finley, New J. Phys. **11**, 023034 (2009).
[22]M. Weiß, S. Kapfinger, T. Reichert, J. J. Finley, A. Wixforth, M. Kaniber, and H. J. Krenner, Appl. Phys. Lett. **109**, 033105 (2016).
[23]R. S. Weis and T. K. Gaylord, Appl. Phys. A **37**, 191 (1985).
[24]D. Royer and E. Dieulesaint, *Elastic Waves in Solids II: Generation, Acousto-Optic Interaction, Applications* (Springer, Berlin/Heidelberg, 2000).
[25]R. Manenti, M. J. Peterer, A. Nersisyan, E. B. Magnusson, A. Patterson, and P. J. Leek, Phys. Rev. B **93**, 041411 (2016).
[26]D. P. Morgan, *Surface Acoustic Wave Filters: With Applications to Electronic Communications and Signal Processing*, 2nd ed. (Academic Press, Amsterdam, 2007).
[27]E. Yablonovitch, D. M. Hwang, T. J. Gmitter, L. T. Florez, and J. P. Harbison, Appl. Phys. Lett. **56**, 2419 (1990).
[28]M. Rotter, C. Rocke, S. Böhm, A. Lorke, A. Wixforth, W. Ruile, and L. Korte, Appl. Phys. Lett. **70**, 2097 (1997).
[29]E. D. S. Nysten, Y. H. Huo, H. Yu, G. F. Song, A. Rastelli, and H. J. Krenner, J. Phys. D: Appl. Phys. **50**, 43LT01 (2017).
[30]J. Pustiowski, K. Müller, M. Bichler, G. Koblmüller, J. J. Finley, A. Wixforth, and H. J. Krenner, Appl. Phys. Lett. **106**, 013107 (2015).
[31]E. Yablonovitch, T. Sands, D. M. Hwang, I. Schnitzer, T. J. Gmitter, S. K. Shastry, D. S. Hill, and J. C. C. Fan, Appl. Phys. Lett. **59**, 3159 (1991).
[32]P. Atkinson, E. Zallo, and O. G. Schmidt, J. Appl. Phys. **112**, 054303 (2012).
[33]M. Weiß, J. B. Kinzel, F. J. R. Schülein, M. Heigl, D. Rudolph, S. Morkötter, M. Döblinger, M. Bichler, G. Abstreiter, J. J. Finley, G. Koblmüller, A. Wixforth, and H. J. Krenner, Nano Lett. **14**, 2256 (2014).
[34]M. Weiß, A. L. Hörner, E. Zallo, P. Atkinson, A. Rastelli, O. G. Schmidt, A. Wixforth, and H. J. Krenner, Phys. Rev. Appl. **9**, 014004 (2018).
[35]C. Nguyen, IEEE Trans. Ultrason., Ferroelectr., Freq. Control **54**, 251 (2007).
[36]D. T. Nguyen, C. Baker, W. Hease, S. Sejil, P. Senellart, A. Lemaitre, S. Ducci, G. Leo, and I. Favero, Appl. Phys. Lett. **103**, 241112 (2013).
[37]L. Zhai, M. C. Löbl, J.-P. Jahn, Y. Huo, P. Treutlein, O. G. Schmidt, A. Rastelli, and R. J. Warburton, Appl. Phys. Lett. **117**, 083106 (2020).
[38]C. Wang, M. Zhang, X. Chen, M. Bertrand, A. Shams-Ansari, S. Chandrasekhar, P. Winzer, and M. Lončar, Nature **562**, 101 (2018).
[39]S. Aghaeimeibodi, B. Desiatov, J.-H. Kim, C.-M. Lee, M. A. Buyukkaya, A. Karasahin, C. J. K. Richardson, R. P. Leavitt, M. Lončar, and E. Waks, Appl. Phys. Lett. **113**, 221102 (2018).
[40]L. Shao, M. Yu, S. Maity, N. Sinclair, L. Zheng, C. Chia, A. Shams-Ansari, C. Wang, M. Zhang, K. Lai, and M. Lončar, Optica **6**, 1498 (2019).
[41]W. Jiang, R. N. Patel, F. M. Mayor, T. P. McKenna, P. Arrangoiz-Arriola, C. J. Sarabalis, J. D. Witmer, R. van Laer, and A. H. Safavi-Naeini, Optica **6**, 845 (2019).
[42]I. Aharonovich, D. Englund, and M. Toth, Nat. Photonics **10**, 631 (2016).
[43]M. Weiß, D. Wigger, M. Nägele, K. Müller, J. J. Finley, T. Kuhn, P. Machnikowski, and H. J. Krenner, arXiv:1910.12949 (2019).
[44]A. Vogele, M. M. Sonner, B. Mayer, X. Yuan, M. Weiß, E. D. S. Nysten, S. F. Covre da Silva, A. Rastelli, and H. J. Krenner, Adv. Quantum Technol. **3**, 1900102 (2020).